Stability of Lithium Superoxide LiO 2 in the Gas Phase: Computational Study of Dimerization and Disproportionation Reactions

ARTICLE *in* THE JOURNAL OF PHYSICAL CHEMISTRY A · AUGUST 2010

Impact Factor: 2.69 · DOI: 10.1021/jp1047584 · Source: PubMed

3 AUTHORS:

Vyacheslav S Bryantsev
Oak Ridge National Laboratory
77 PUBLICATIONS **2,242** CITATIONS
SEE PROFILE

Mario Blanco
King Abdullah University of Science and Te…
64 PUBLICATIONS **1,705** CITATIONS
SEE PROFILE

Francesco Faglioni
Università degli Studi di Modena e Reggio …
35 PUBLICATIONS **1,015** CITATIONS
SEE PROFILE

Stability of Lithium Superoxide LiO_2 in the Gas Phase: Computational Study of Dimerization and Disproportionation Reactions

Vyacheslav S. Bryantsev,*,† Mario Blanco,† and Francesco Faglioni†,‡

Liox Power, Incorporated, 129 North Hill Avenue, Suite 103, Pasadena, California 91106 and Dipartimento di Chimica, Università di Modena e Reggio Emilia, Via Campi 183, 41100 Modena, Italy

Received: May 24, 2010

Knowledge of the precise molecular mechanisms during the discharge and recharge processes in the lithium−air battery is critical for achieving desired improvements in specific capacity, current density, and cyclability. The initial oxygen reduction product formed in the presence of Li^+ ions is lithium superoxide LiO_2. In this study, we report the computed structures and thermodynamic parameters of LiO_2 dimerization in the gas phase, which enables us to provide a baseline for the reaction free energy profile of the subsequent disproportionation of $(LiO_2)_2$ to lithium peroxide Li_2O_2 and O_2. Our calculations identified several low-lying $(LiO_2)_2$ dimers, with the singlet bipyramidal structure giving IR bands that are consistent with the characteristic IR vibration frequencies of $(LiO_2)_2$ in the oxygen matrix at $T = 15-40$ K. The activation barrier for $(LiO_2)_2 = Li_2O_2+O_2$ is 10.9 kcal/mol at the UCCSD(T)/CBS level ($T = 298$ K), suggesting that in the gas phase LiO_2 and its aggregates could only be observed at low temperatures.

1. Introduction

There is a recent surge of interest in developing Li/air (oxygen) nonaqueous electrolyte rechargeable batteries that offer high theoretical gravimetric energy densities.[1−17] Although the use of an O_2 cathode could increase the practical gravimetric energy density by a factor of 5−10, compared to conventional rechargeable lithium-ion batteries,[18] the realization of a practical rechargeable Li−air cell poses a significant challenge. Lack of knowledge of the precise molecular mechanisms during discharge and recharge processes may hamper further progress in achieving desired specific capacity along with sufficient power density and cycle life for battery applications.

The superoxide ion, O_2^-, plays an essential role in the chemistry of oxygen reduction in nonaqueous aprotic solvents and in room temperature ionic liquids.[19−23] The electrochemical response of the O_2/O_2^- redox couple on a particular electrode is dependent on the solvent and nature of the counterion.[24,25] Typically, oxygen reduction is reversible in the presence of large and bulky counterions, such as tetrabutylammonium, but highly irreversible in the presence of small counterions, such as lithium, because of the low stability of LiO_2 and subsequent passivation of the electrode surface by solid lithium peroxide or lithium oxide products. Still, it has been reported that LiO_2 has a finite lifetime on the glassy carbon electrode surface.[24,25] Depending on the potential scan rate during cyclic voltammetry, LiO_2 can be either further electrochemically reduced to Li_2O_2 or chemically decomposed to lithium peroxide Li_2O_2 and O_2 via a disproportionation reaction.

Since the LiO_2 molecule was prepared by Andrews at low temperatures ($T = 15-40$ K) in inert and oxygen matrices,[26] it has been extensively studied using infrared (IR),[27,28] Raman,[28,29] electronic,[30] electron spin resonance,[31] and soft-X-ray spectroscopies[32] as well as theoretical calculations at various levels of theory.[27,33−38] The majority of previous studies, however, were limited to the characterization of physicochemical properties and bonding in LiO_2, whereas the thermodynamic and chemical stability of LiO_2 and its aggregates, including dimerization, has not been explored in much detail.

We report the computed structures and thermodynamic parameters of LiO_2 dimerization in the gas phase, which enables us to study the reaction free energy profile for the subsequent disproportionation (decomposition) of $(LiO_2)_2$ to Li_2O_2 and O_2. The presence of $(LiO_2)_2$ in the pure O_2 matrix experiments has been hypothesized from the analysis of IR bands upon sample warming and by variation in Li and O_2 concentration.[26] Although several IR bands were assigned to the LiO_2 dimer, these earlier studies had no direct experimental structural data to support the spectral assignment. Here, we employ high-level quantum chemical calculations to relate these spectroscopic measurements to the chemical structure of the dimer and determine the role of thermodynamics and kinetic barriers in the chemical decomposition of the $(LiO_2)_2$ adduct.

2. Computational Methods

Electronic structure calculations were carried out using the Jaguar 7.5[39] and NWChem 5.1[40] programs. We used the B3LYP[41,42] flavor of density functional theory (DFT) in the 6-311++G** basis set to calculate the geometries, IR frequencies, and thermodynamic data for $(LiO_2)_2$ complexes in several binding motifs (Figures 1−4 and Tables 1−4). We used the recommended[43] scaling factor (0.9679) for fundamental vibrational frequencies calculated with the B3LYP/6-311++G** method. The standard Gibbs free energy of each species in the gas phase ($T = 298$ K, $P = 1$ atm) was calculated using the rigid rotor-harmonic oscillator approximation. Here, no frequency scaling was necessary, because applying the recommended scaling factors for low-frequency vibrations (1.0100) and zero-point vibration energies (0.9877) resulted in very small changes in the reaction free energies (<0.015 kcal/mol) compared to those given in Table 4.

* To whom correspondence should be addressed. Phone: (626) 389 6306. Fax: (626) 389 6302. E-mail: slava@liox.com.
† Liox Power, Inc.
‡ Università di Modena e Reggio Emilia.

10.1021/jp1047584
Published on Web 07/16/2010

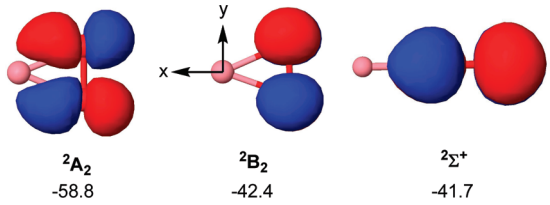

Figure 1. Highest doubly-occupied molecular orbitals (β-spin HOMOs) for LiO_2 in the $^2A_2$, $^2B_2$, and $^2\Sigma^+$ electronic states and O_2 electronic binding energies (kcal/mol) at the B3LYP/6-311++G** level. MOs are rendered at 0.05 $(e/Å^3)^{1/2}$ isovalues.

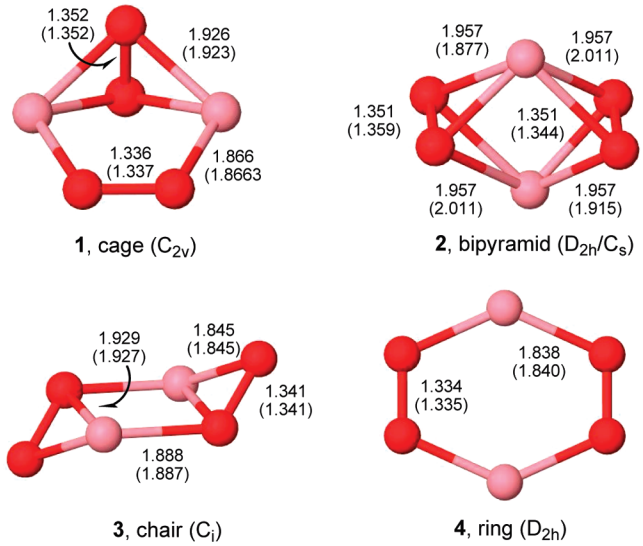

Figure 2. Structures of four low-lying $(LiO_2)_2$ isomers. O−O and Li−O bond lengths for the lowest singlet and triplet (in parentheses) states obtained with B3LYP/6-311++G** are shown.

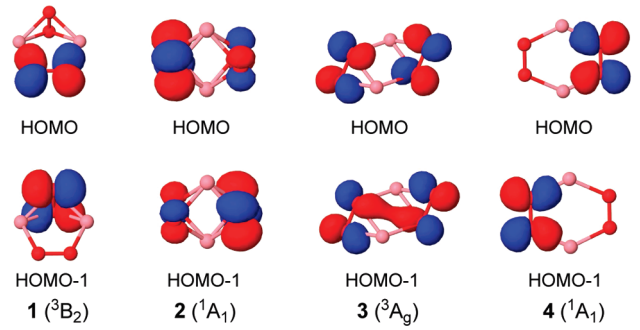

Figure 3. Highest doubly-occupied molecular orbitals (β-spin HOMOs) for **1**−**4** in the ground electronic states at the B3LYP/6-311++G** level. The orientation of the occupied O_2^- π^* orbitals is such as to maximize their electrostatic interaction with lithium ions. MOs are rendered at 0.05 $(e/Å^3)^{1/2}$ isovalues.

For $(LiO_2)_2$ dimers we also performed single-point energy calculations on B3LYP/6-311++G**-optimized geometries using coupled-cluster theory with single, double, and perturbative triple excitations[44−46] for unrestricted (UHF) reference wave functions [UCCSD(T)/aug-cc-pVTZ]. In addition, reaction energies for $(LiO_2)_2$ disproportionation along the lowest free energy path were obtained at the complete basis set limit (CBS) of the UMP2 theory.[47] For the basis set expansion in our UMP2 calculations, we used a family of augmented correlation-consistent basis sets[48,49] (aug-cc-pV*n*Z, n = T, Q, 5). Only the valence electrons were correlated in the UMP2 calculations. The largest basis set for geometry optimization was aug-cc-pVTZ.

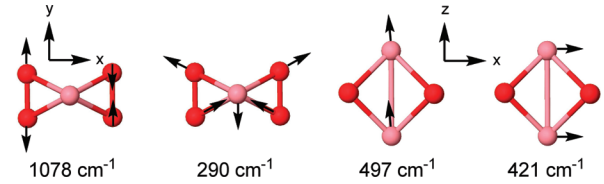

Figure 4. Calculated infrared active normal modes of vibration of the singlet bipyramidal $(LiO_2)_2$ molecule.

TABLE 1: Comparison of the Experimetal and Calculated Harmonic Frequencies (cm^{-1}) and Infrared intensities (km/mol) of the $^2A_2$ LiO_2 (C_{2v} structure) and ^1A_g Li_2O_2 (D_{2h} structure) Molecules

B3LYP, ref 27, freq. (int.)[a]	B3LYP, this work, freq. (int.)[b]	mode	expt[a]
	lithium superoxide LiO_2		
527.9 (31)	508.9 (28)	B_2, antisym Li−O	508.9
753.3 (117)	719.7 (124)	A_1, sym Li−O	719.7
1175.4 (9)	1093.9 (10)	A_1, sym O−O	1093.9
	lithium peroxide Li_2O_2		
61 (184)	65.1 (194)	B_{1u}, out of plane	298 (argon)[c]
456.6 (174)	430.6 (179)	B_{3u}, antisym Li−O	455.1
610.7 (0)	580.8 (0)	B_{1g}, sym Li−O	
665.6 (0)	629.0 (0)	A_g, sym Li−O	
834.3 (0)	794.5 (0)	A_g, sym Li−O	
847.7 (326)	818.2 (341)	B_{2u}, antisym Li−O	810.4

[a] Infrared spectra for ^7Li atoms and $^{16}O_2$ molecules in excess neon at 5 K.[27] Density functional calculations were done for these isotopes at the B3LYP/6-311+G(3df) level.[27] [b] Obtained at the B3LYP/6-311++G** level using the scaling factor of 0.9679. [c] Reference 26.

TABLE 2: Relative Electronic Energies (with and without zero-point-energy (ZPE) corrections) and Standard Gibbs Free Energies (kcal/mol) for $(LiO_2)_2$ 1−4 Calculated with UCCSD(T) and B3LYP Methods

			no. of imaginary	B3LYP[b]	UCCSD(T)[c]		
dimer	sym	state	frequencies[a]	ΔE_e	ΔE_e	ΔE_e + ZPE	ΔG^{od}
1	C_{2v}	$^3B_2$	0	0.00	**0.00**	**0.00**	**0.00**
1	C_{2v}	$^1B_2$	0	0.31	**0.20**	**0.21**	**1.17**
2	C_s	$^3A'$	1	4.41	3.31	2.45	2.50
2	D_{2h} (C_{2v})[e]	$^1A_1$	0	2.31	**0.63**	**0.33**	1.67
3	C_i	^3A_g	0	0.45	1.35	1.43	**0.85**
3	C_i (C_1)[f]	^1A	0	0.47	1.32	1.42	1.50
4	D_{2h}	$^3B_{2u}$	1	3.16	5.14	4.75	4.56
4	D_{2h} (C_{2v})[e]	$^1A_1$	1	3.04	5.09	4.72	4.83

[a] The number of imaginary frequencies. [b] Optimized with B3LYP/6-311++G**. Singlet-state wave functions have M_s = 0 (equal number of α and β spins) in which α and β spins are located on different orbitals. [c] UCCSD(T)/aug-cc-pVTZ single-point energies on B3LYP/6-311++G**-optimized geometries. The three lowest energy states are shown in bold. [d] ZPE and thermal corrections are calculated at the B3LYP/6-311++G** level. [e] The molecule has D_{2h} point-group symmetry, but the symmetry of singly occupied orbitals is C_{2v}. [f] The molecule has C_i point-group symmetry, but the symmetry of singly occupied orbitals is C_1.

To estimate the UMP2 CBS limit of the dimerization energy, we utilized an extrapolation scheme based on a polynomial function of inverse powers of 4 and 5[50,51]

$$\Delta E(n) = \Delta E_{CBS} + B/(l_{max} + 1)^4 + C/(l_{max} + 1)^5 \quad (1)$$

where n = 3, 4, 5 for n = T, Q, and 5 in aug-cc-pVnZ, respectively, and ΔE_{CBS}, B, and C are the fitting parameters. The UCCSD(T)/

TABLE 3: Comparison of the Calculated Harmonic Frequencies (cm^{-1}) and Infrared Intensities (km/mol) of Several $(LiO_2)_2$ Molecules with the Observed Infrared Absorbtions Attributed to $(LiO_2)_2$[a]

1 ($^3B_2$)	**1** ($^1B_2$)	**3** (^3A_g)	**3** (^1A_g)	**4** ($^1A_1$)	**2** ($^1A_1$)		
freq. (int.)	freq. (int.)	freq. (int.)	freq. (int.)	freq. (int.)	freq. (int.)	mode	expt[a]
89.0 (0)	119.9 (0)	91.4 (9)	87.4 (10)	−56.1	**173.1 (31)**	out-of-plane OLiLiO′	
174.0 (19)	159.7 (18)	111.1 (0)	104.5 (0)	82.3 (18)	**195.5 (22)**	OO···O′O′ twisting	
191.4 (56)	192.2 (54)	166.1 (69)	165.2 (70)	82.5 (42)	**218.4 (0)**	in-plane sym OO···O′O′ stretch	
199.6 (6)	201.7 (7)	267.5 (0)	264.8 (0)	133.4 (0)	**234.3 (0)**	OO···O′O′ wagging	
257.1 (66)	250.9 (69)	277.7 (0)	278.7 (0)	195.1 (187)	**289.2 (0)**	in-plane anti OO···O′O′ stretch	
282.6 (0)	277.3 (0)	309.4 (84)	308.4 (82)	213.3 (0)	**290.2 (37)**	in-plane anti OO···O′O′ stretch	351
476.1 (209)	472.4 (211)	387.2 (212)	384.8 (214)	420.7 (0)	**349.0 (0)**	anti Li−O−Li stretch	
501.8 (11)	500.1 (9)	481.3 (0)	478.7 (0)	445.6 (173)	**420.7 (139)**	sym Li−O−Li stretch	
526.7 (17)	522.3 (17)	559.7 (0)	559.5 (0)	636.0 (0)	**497.2 (252)**	Li−O−Li rocking	521
568.5 (221)	567.2 (231)	641.7 (263)	641.9 (268)	666.5 (242)	**534.7 (0)**	Li−O−Li scissoring	
1116.1 (3)	1117.6 (2)	1152.4 (22)	1153.3 (22)	1188.0 (0)	**1078.2 (102)**	anti O−O stretch	1048
1174.4 (3)	1176.9 (2)	1155.1 (0)	1154.8 (0)	1190.0 (7)	**1121.1 (0)**	sym O−O stretch	

[a] Infrared absorption peaks in the pure O_2 matrix observed in addition to the bands assigned to LiO_2.[26] The calculated infrared spectrum of the singlet bipyramidal dimer **2** that agrees with the experimental results is in bold.

TABLE 4: Changes in Reaction Energies for the Disproportionation of Two LiO_2 Radicals to Li_2O_2 and O_2 (kcal/mol); the Reference Energy Is That of the Isolated LiO_2 Radical[a]

method	$(LiO_2)_2$, **1** triplet	LiO_2LiO_2-TS triplet	LiO_2LiO_2 triplet	LiO_2LiO_2 singlet	Li_2O_2 + O_2 triplet
B3LYP/6-311++G** (B3LYP)	−34.71	−25.77	−25.99	−23.17	−15.63
UMP2/aug-cc-pVTZ (UMP2)	−35.96	−23.13	−24.32	−24.33	−22.34
UMP2/aug-cc-pVQZ	−35.63	−22.75	−23.93	−23.95	−22.35
UMP2/aug-cc-pV5Z	−35.44	−22.55	−23.71	−23.71	−22.34
UMP2/CBS[b]	−35.21	−22.30	−23.41	−23.38	−22.34
UCCSD(T)/aug-cc-PVTZ//B3LYP[c]	−35.42	−17.62	−15.94	−20.50	−18.87
UCCSD(T)/aug-cc-PVTZ//UMP2[d]	−35.37	−22.62	−23.98	−24.00	−18.72
UCCSD(T)/CBS[e]	−34.62	−21.79	−23.07	−23.05	−18.71
UCCSD(T)/CBS + ZPE[f]	−33.53	−21.22	−22.63	−22.45	−18.40
UCCSD(T)/CBS + ZPE + $\Delta G_{0\rightarrow 298}$[f]	−23.55	−12.73	−14.78	−13.13	−16.88

[a] Reaction free energy profile obtained at the UCCSD(T) level and structures of the complexes optimized at the UMP2/aug-cc-pVTZ level are shown in Figure 5. [b] To estimate the UMP2/CBS limit of the interaction energy, we utilized the extrapolation scheme defined by eq 1.[50,51] [c] UCCSD(T)/aug-cc-pVTZ single-point energies on B3LYP/6-311++G**-optimized geometries. [d] UCCSD(T)/aug-cc-pVTZ single-point energies on UMP2/aug-cc-pVTZ-optimized geometries. [e] The UCCSD(T)/CBS limit is estimated using eqs 2a and 2b. [f] ZPE and thermal corrections are calculated at the B3LYP/6-311++G** level.

CBS reaction energies and barrier heights were estimated by combining the UMP2/CBS energies with UCCSD(T)/aug-cc-pVTZ corrections[52,53]

$$\Delta E_e(\text{UCCSD(T)/CBS}) = \Delta E_e(\text{UMP2/CBS}) + \delta\text{UCCSD(T)} \quad (2a)$$

$$\delta\text{UCCSD(T)} = \Delta E_e(\text{UCCSD(T)/aug-cc-pVTZ}) - \Delta E_e(\text{UMP2/aug-cc-pVTZ}) \quad (2b)$$

3. Results and Discussion

We first consider the LiO_2 radical, in which O_2 is strongly bound (ΔE_e = 58.8 and 58.3 kcal/mol at the B3LYP and UCCSD(T) levels of theory, respectively) in the side-on (η^2) coordination geometry ($^2A_2$ state in C_{2v} symmetry in Figure 1). Binding in an η^2 fashion results in the predominantly ionic three-centered bond between the Li^+ cation and the O_2^- anion−radical π^* orbital oriented in the molecular plane (π^*_{xy}), leaving the second π^* orbital singly occupied (π^*_{yz}).

The side-on binding of O_2^- to Li^+ might occur through the electrostatic interaction with the O_2^- π^*_{yz} orbital perpendicular to the molecular plane ($^2B_2$ state in C_{2v} symmetry in Figure 1). However, we find that this interaction leads to a bond strength of 42.4 kcal/mol at the B3LYP level, which is 16.4 kcal/mol smaller than that for the $^2A_2$ state. We were also able to find a stable linear (end-on) complex ($^2\Sigma^+$ state in Figure 1), but this was bound by only 41.7 kcal/mol at the B3LYP level. The symmetric binding of superoxide is favorable, because it maximizes the electrostatic interaction with the lithium ion. This contrasts with the case of transition metal−dioxygen compounds, where the strong interaction of O_2^- π^* orbitals with the metal d orbitals typically leads to superoxo complexes in the end-on (η^1) geometry.[54,55]

Table 1 shows the comparison of the experimental and calculated harmonic frequencies for LiO_2 and Li_2O_2 molecules.

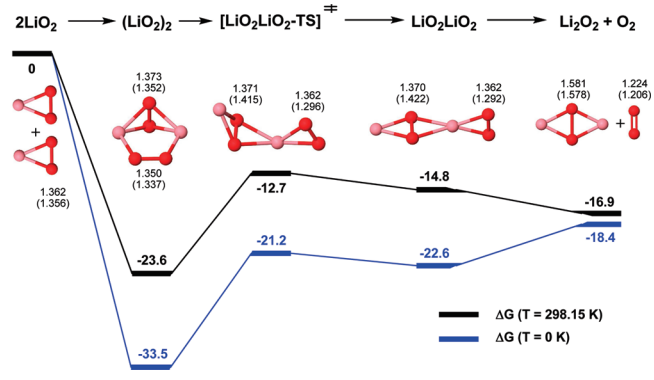

Figure 5. Reaction free energy profile (T = 0 and 298.15 K) for the disproportionation of the LiO_2 molecules to Li_2O_2 and O_2 (kcal/mol) obtained for the triplet LiO_2 dimer species at the UCCSD(T)/CBS level. Structures are optimized using the UMP2/aug-cc-pVTZ method. O−O bond lengths obtained with B3LYP/6-311++G** are shown in parentheses.

The O−O stretching frequencies of ~1100 and ~800 cm^{-1} are within the typical range observed for the superoxo and peroxo complexes, respectively.[54,55] Consistent with previous DFT calculations,[27] B3LYP frequencies after scaling agree closely with experiment (an average error of 15 cm^{-1}).

Structures of the four low-lying isomers of $(LiO_2)_2$ and selected geometrical parameters for the lowest energy singlet and triplet states are depicted in Figure 2. Relative energies of these complexes are summarized in Table 2. In what follows, we discuss relative energies obtained at the UCCSD(T) level at 0 K with the effects of zero-point energy included. The cage isomer (**1**) in its triplet state is the most stable dimer, followed by the singlet state of the same type, which is only 0.2 kcal/mol higher in energy. The singlet bipyramidal structure (**2**) is the third lowest energy state, which is also only marginally higher in energy (by 0.3 kcal/mol) than the most stable form. Chair (**3**) (1.4 kcal/mol) and ring (**4**) (4.7 kcal/mol) isomers are less stable geometries. The chair complex is a local minimum, while the planar ring complex exhibits one imaginary frequency at the B3LYP level. A relatively small difference in the energies of the singlet and triplet states for each dimer type is indicative of a weak magnetic interaction between the unpaired spins. The notable exception is a singlet ground state of the bipyramid dimer that exhibits a singlet−triplet gap of 2.1 kcal/mol. Ferromagnetic coupling in **2** (triplet state) lowers the molecular symmetry from D_{2h} to C_s and changes the nature of the stationary point from a minimum to a transition state, which corresponds to rotation of one of the oxygen molecules in **1** along the symmetry axis. Examination of the shapes of HOMOs in the ground electronic state of these mainly ionic systems further confirms that O_2^- π^* orbitals are oriented to maximize the electrostatic interaction with a positive charge on each lithium center (Figure 3).

Table 3 compares the calculated harmonic frequencies of stable $(LiO_2)_2$ dimers with the observed infrared absorption bands assigned to a dimer.[26] The singlet ground state of dimer **4** was also included because it is a local minimum at the UMP2/aug-ccpVTZ level. The most characteristic feature in the IR spectrum of a dimer is a single O−O stretching absorption band at 1048 cm^{-1}, which is 49 cm^{-1} red shifted compared to that of LiO_2. Analysis of data from Table 3 shows that the calculated spectrum of dimer **2** nicely reproduces this spectral signature and matches the experimental data at the low-frequency region quite well. Identification of the calculated vibrational modes for this dimer (Table 3 and Figure 4) allows unambiguous assignment of the observed bands. Isotopic substitution indicated that the band at 521 cm^{-1} exhibits a large (27 cm^{-1}) lithium isotopic shift and a small oxygen isotopic shift (6 cm^{-1}),[26] consistent with the rocking mode vibration of two Li atoms. The band at 351 cm^{-1} has moderate lithium (9 cm^{-1}) and oxygen (12 cm^{-1}) isotopic shifts,[26] which are assigned to in-plane antisymmetric OO···O′O′ stretching coupled with the lithium motion in the perpendicular plane (Figure 4). In contrast, the calculated spectral signatures of dimers **1**, **3**, and **4** do not appear to be consistent with the experiment. For example, dimers **3** and **4** exhibit O−O stretching bands at frequencies much higher than that of LiO_2, while dimer **1** has two infrared-active O−O stretching modes, although of low intensity.

The results presented above provide conclusive evidence that the low-temperature IR spectrum corresponds to dimer **2**. Although ab initio calculations predict the cage dimer **1** to be lower in energy, the energetic difference is only 0.3 kcal/mol at $T = 0$ K, which is below the accuracy of calculations. It should be noted, however, that the relative stability of the triplet state **1**($^3B_2$) increases with temperature, and this form becomes 1.7 kcal/mol more stable than the singlet state **2**($^1A_1$) at standard conditions ($T = 298$ K), as indicated in the last column of Table 2. Therefore, we chose the computationally more stable cage dimer **1** as an initial geometry for the disproportionation reaction and assumed that all reaction participants are in their triplet states. Control calculations for a singlet LiO_2LiO_2 intermediate shown in Table 4 confirm that this form is 1.6 kcal/mol less stable than the triplet form at 298 K. Focusing on triplet states also ensures that the formation of triplet oxygen is a spin-allowed process, which is expected to be much faster than that involving intersystem crossing from the singlet potential-energy surface to the triplet one.

The proposed reaction mechanism for the disproportionation of LiO_2 is depicted in Figure 5, and reaction energies at various levels of theory are given in Table 4. Structures of the complexes shown in Figure 5 are optimized at the UMP2/aug-cc-pVTZ level. First, a stable $(LiO_2)_2$ dimer is formed. Next, a stable intermediate LiO_2LiO_2 forms by a mechanism involving the abstraction of a lithium ion from one of the superoxides. This rate-determining step proceeds through the late transition state with a barrier of 10.9 kcal/mol in the forward direction and a barrier of 4.2 kcal/mol in the backward direction. In the final step, LiO_2LiO_2 breaks down into LiO_2Li and O_2, which is an enthalpically disfavored but free energy favored process at $T = 298$ K. For fast dissociative processes, transition states can be accurately defined only on the free energy hypersurface, which we have not attempted to determine here. The endothermicity of the dissociation step at 0 K implies that the overall reaction barrier could be larger at very low temperatures.

The results shown in Figure 5 indicate that the $(LiO_2)_2$ dimer is thermodynamically more stable than $Li_2O_2 + O_2$ at both 0 and 298 K. Thus, at very low LiO_2 concentrations (high dilution of Li atoms in oxygen matrix) the disproportionation of $(LiO_2)_2$ will not occur. This is consistent with the observation that no Li_2O_2 is detected in the pure O_2 matrix experiments with a O_2/Li concentration ratio of 300−1000.[26] However, the thermodynamic stability of the disproportionation product will increase if Li_2O_2 molecules can aggregate. In the limit of infinite crystal size, the thermodynamic stability of LiO_2(solid) compared to Li_2O_2(solid) at an oxygen pressure of 1 atm can be estimated from the recent DFT calculations employing the generalized gradient approximation (PW91).[56] In this work Seriani[56] reported the formation energies (with respect to lithium and molecular oxygen) of the hexagonal structure of Li_2O_2 (*P*63/*mmc* space group) and the most stable orthorhombic structure of LiO_2 (*Pnnm* space group). The calculated free energy of formation of Li_2O_2 was underestimated compared to experiment by 21.7 kcal/mol.[56] A similar error for the formation free energy of Li_2O_2 (22.6 kcal/mol) has been recently reported by Hummelshøj[57] using the RPBE exchange correlation functional. Keeping in mind this caveat, the Li_2O_2 structure was predicted[56] to be more stable than the $2LiO_2$ stoichiometry by 8.3 kcal/mol at 0 K (without zero-point energy corrections). Taking into account the entropy of molecular oxygen at $T = 298$ K and $p_{O2} = 1$ atm (49.03 cal mol^{-1} K^{-1}),[58] the estimated standard reaction free energy for $2LiO_2$(solid) = Li_2O_2(solid) + O_2(gas) is −22.9 kcal/mol. Thus, there is a strong thermodynamic driving force to form Li_2O_2 crystals at all temperatures. This fact combined with a small activation barrier for the disproportionation reaction in the gas phase indicates that the bulk LiO_2 phase would be unstable. This is consistent with the fact that there are no experimental reports on the crystal structure of LiO_2[56] and also

explains why O_2 evolution is often seen as an indication of disproportionation.[24]

Energy differences between various oxides and reaction energies obtained from high-accuracy electronic structure calculations at the UCCSD(T)/CBS level can serve as a reliable benchmark for evaluating the accuracy of computationally less demanding DFT methods. The results presented in Tables 1 and 4 suggest that B3LYP provides an adequate description of relative energies of lithium oxides of various compositions, with typical errors below 3 kcal/mol. The largest error of B3LYP is for the TS barrier height, which is underestimated by ~4 kcal/mol. B3LYP predicts O−O bond lengths of stable species to within 0.02−0.07 Å (Figure 5) of the values at the UMP2 level. Again, the largest discrepancy is for a TS structure (LiO_2LiO_2-TS) and a high-energy intermediate (LiO_2LiO_2) that are incorrectly predicted to have a partial charge transfer from one oxygen molecule to another at the B3LYP level (one O−O bond is longer than the other by >0.1 Å).

4. Conclusions

Our calculations found several low-lying $(LiO_2)_2$ dimers and identified the singlet bipyramidal structure as the one giving IR bands that are consistent with the characteristic IR vibration frequencies of $(LiO_2)_2$ in the oxygen matrix at $T = 15-40$ K. An activation barrier for $(LiO_2)_2 = Li_2O_2 + O_2$ at standard conditions is predicted to be 10.9 kcal/mol at the UCCSD(T)/CBS level, suggesting that in the gas phase LiO_2 species and its aggregates could only be observed at low temperatures. This is consistent with experiment. This study provides important basic knowledge to further understanding the chemical transformations of LiO_2 in organic condensed phase solutions, which will be the scope of our next work.

Acknowledgment. We are grateful to Gregory Chase and Dan Addison for helpful discussions.

References and Notes

(1) Abraham, K. M.; Jiang, Z. A. *J. Electrochem. Soc.* **1996**, *143*, 1–5.
(2) Read, J. *J. Electrochem. Soc.* **2002**, *149*, A1190–A1195.
(3) Read, J.; Mutolo, K.; Ervin, M.; Behl, W.; Wolfenstine, J.; Driedger, A.; Foster, D. *J. Electrochem. Soc.* **2003**, *150*, A1351–A1356.
(4) Kuboki, T.; Okuyama, T.; Ohsaki, T.; Takami, N. *J. Power Sources* **2005**, *146*, 766–769.
(5) Ogasawara, T.; Débart, A.; Holzapfel, M.; Novák, P.; Bruce, P. G. *J. Am. Chem. Soc.* **2006**, *128*, 1390–1393.
(6) Read, J. *J. Electrochem. Soc.* **2006**, *153*, A96–A100.
(7) Kowalczk, I.; Read, J.; Salomon, M. *Pure Appl. Chem.* **2007**, *79*, 851–860.
(8) Mirzaeian, M.; Hall, P. J. *Power System Technol.* **2007**, *31*, 90–96.
(9) Débart, A.; Bao, J.; Armstrong, G.; Bruce, P. G. *J. Power Sources* **2007**, *174*, 1177–1182.
(10) Débart, A.; Paterson, A. J.; Bao, J.; Bruce, P. G. *Angew. Chem., Int. Ed.* **2008**, *47*, 4521–4524.
(11) Yang, X.-H.; He, P.; Xia, Y.-Y. *Electrochem. Commun.* **2009**, *11*, 1127–1130.
(12) Beattie, S. D.; Manolescu, D. M.; Blair, S. L. *J. Electrochem. Soc.* **2009**, *156*, A44–A47.
(13) Xu, W.; Xiao, J.; Zhang, J.; Wang, D.; Zhang, J.-G. *J. Electrochem. Soc.* **2009**, *156*, A773–A779.
(14) Yang, X.-H.; Xia, Y.-Y. *J. Solid State Electrochem.* **2010**, *14*, 109–114.
(15) Tran, C.; Yang, X.-Q.; Qu, D. *J. Power Sources* **2010**, *195*, 2057–2063.
(16) Kumar, B.; Kumar, J.; Leese, R.; Fellner, J. P.; Rodrigues, S. J.; Abraham, K. M. *J. Electrochem. Soc.* **2010**, *157*, A50–A54.
(17) Xu, W.; Xiao, J.; Wang, D.; Zhang, J.; Zhang, J.-G. *J. Electrochem. Soc.* **2010**, *157*, A219–A224.
(18) Armand, M.; Tarascon, J.-M. *Nature* **2008**, *451*, 652–657.
(19) Sawyer, D. T. *Oxygen Chemistry*; Oxford University Press: New York, 1991.
(20) Andrieux, C. P.; Hapiot, P.; Savéant, J.-M. *J. Am. Chem. Soc.* **1987**, *109*, 3768–3775.
(21) Islam, M. M.; Ohsaka, T. *J. Phys. Chem. C* **2008**, *112*, 1269–1275.
(22) René, A.; Hauchard, D.; Lagrost, C.; Hapiot, P. *J. Phys. Chem. B* **2009**, *113*, 2826–2831.
(23) Huang, X.-J.; Rogers, E. I.; Hardacre, C.; Compton, R. G. *J. Phys. Chem. B* **2009**, *113*, 8953–8959.
(24) Laoire, C. O.; Mukerjee, S.; Abraham, K. M.; Plichta, E. J.; Hendrickson, M. A. *J. Phys. Chem. C* **2009**, *113*, 20127–20134.
(25) Laoire, C. O.; Mukerje, S.; Abraham, K. M.; Plichta, E. J.; Hendrickson, M. A. *J. Phys. Chem. C* **2010**, *114*, 9178–9186.
(26) Andrews, L. *J. Chem. Phys.* **1969**, *50*, 4288–4299.
(27) Wang, X.; Andrews, L. *Mol. Phys.* **2009**, *107*, 739–748.
(28) Hatzenbuhler, D. A.; Andrews, L. *J. Chem. Phys.* **1972**, *56*, 3398–3403.
(29) Andrews, L.; Smardzewski, R. R. *J. Chem. Phys.* **1973**, *58*, 2258–2261.
(30) Andrews, L. *J. Mol. Spectrosc.* **1976**, *61*, 337–345.
(31) Lindsay, D. M.; Garland, D. A. *J. Phys. Chem.* **1987**, *91*, 6158–6161.
(32) Qiu, S. L.; Lin, C. L.; Chen, J.; Strongin, M. *Phys. Rev. B* **1989**, *39*, 6194–6197.
(33) Allen, W. D.; Horner, D. A.; Dekock, R. L.; Remington, R. B.; Schaefer, H. F., III *Chem. Phys.* **1989**, *133*, 11–45.
(34) Partridge, H.; Bauschlicher, C. W.; Sodupe, M.; Langhoff, S. R. *Chem. Phys. Lett.* **1992**, *195*, 200–206.
(35) Bauschlicher, C. W.; Sodupe, M.; Partridge, H.; Langhoff, S. R. *Chem. Phys. Lett.* **1992**, *197*, 213–216.
(36) Bruna, P. J.; Grein, F. *J. Phys. Chem. A* **1999**, *103*, 3294–3301.
(37) Bruna, P. J.; Grein, F. *Mol. Phys.* **1999**, *97*, 321–328.
(38) Yang, Z. J.; Gao, Q. H.; Guo, Y. D.; Cheng, X. L.; Zhu, Z. H.; Yang, X. D. *Acta Phys. Sin.* **2007**, *56*, 5723–5726.
(39) *Jaguar*, version 7.5; Schrödinger, LLC: New York, 2008.
(40) Bylaska, E. J.; de Jong, W. A.; Govind, N.; Kowalski, K.; Straatsma, T. P.; Valiev, M.; Wang, D.; Apra, E.; Windus, T. L.; Hammond, J.; Nichols, P.; Hirata, S.; Hackler, M. T.; Zhao, Y.; Fan, P.-D.; Harrison, R. J.; Dupuis, M.; Smith, D. M. A.; Nieplocha, J.; Tipparaju, V.; Krishnan, M.; Wu, Q.; Van Voorhis, T.; Auer, A. A.; Nooijen, M.; Brown, E.; Cisneros, G.; Fann, G. I.; Fruchtl, H.; Garza, J.; Hirao, K.; Kendall, R.; Nichols, J. A.; Tsemekhman, K.; Wolinski, K.; Anchell, J.; Bernholdt, D.; Borowski, P.; Clark, T.; Clerc, D.; Dachsel, H.; Deegan, M.; Dyall, K.; Elwood, D.; Glendening, E.; Gutowski, M.; Hess, A.; Jaffe, J.; Johnson, B.; Ju, J.; Kobayashi, R.; Kutteh, R.; Lin, Z.; Littlefield, R.; Long, X.; Meng, B.; Nakajima, T.; Niu, S.; Pollack, L.; Rosing, M.; Sandrone, G.; Stave, M.; Taylor, H.; Thomas, G.; van Lenthe, J.; Wong, A.; Zhang, Z. *NWChem, A Computational Chemistry Package for Parallel Computers*, Version 5.1; Pacific Northwest National Laboratory: Richland, WA, 2007.
(41) Becke, A. D. *Phys. Rev. A* **1988**, *38*, 3098–3100.
(42) Lee, C. T.; Yang, W. T.; Parr, R. G. *Phys. Rev. B* **1988**, *37*, 785–789.
(43) Andersson, M. P.; Uvdal, P. *J. Phys. Chem. A* **2005**, *109*, 2937–2941.
(44) Purvis, G. D.; Bartlett, R. J. *J. Chem. Phys.* **1982**, *76*, 1910–1918.
(45) Raghavachari, K.; Trucks, G. W.; Pople, J. A.; Head-Gordon, M. *Chem. Phys. Lett.* **1989**, *157*, 479–483.
(46) Watts, J. D.; Gauss, J.; Bartlett, R. J. *J. Chem. Phys.* **1993**, *98*, 8718–8733.
(47) Möller, C.; Plesset, M. S. *Phys. Rev.* **1934**, *46*, 618–622.
(48) Dunning, T. H., Jr. *J. Chem. Phys.* **1989**, *90*, 1007–1023.
(49) Kendall, R. A.; Dunning, T. H., Jr.; Harrison, R. J. *J. Chem. Phys.* **1992**, *96*, 6796–6806.
(50) Xantheas, S. S.; Burnham, C. J.; Harrison, R. I. *J. Chem. Phys.* **2002**, *116*, 1493–1499.
(51) Xantheas, S. S.; Aprá, E. *J. Chem. Phys.* **2004**, *120*, 823–828.
(52) Bates, D. M.; Tschumper, G. S. *J. Phys. Chem. A* **2005**, *109*, 2937–2941.
(53) Bryantsev, V. S.; Diallo, M. S.; van Duin, A. C. T.; Goddard, W. A., III *J. Chem. Theory Comput.* **2009**, *5*, 1016–1026.
(54) Valentine, J. S. *Chem. Rev.* **1973**, *73*, 235–245.
(55) Borovik, A. C.; Zinn, P. G.; Zart, M. K. Dioxygen Binding and Activation: Reactive Intermediates. In *Activation of Small Molecules: Organometallic and Bioinorganic Perspectives*; Tolman, W. B., Ed.; Wiley-VCH GmbH & Co.: KGaA, New York, 2006, *187*234.
(56) Seriani, N. *Nanotechnology* **2009**, *20*, 445703.
(57) Hummelshøj, J. S.; Blomqvist, J.; Datta, S.; Vegge, T.; Rossmeisl, J.; Thygesen, K. S.; Luntz, A. C.; Jacobsen, K. W.; Nørskov, J. K. *J. Chem. Phys.* **2010**, *132*, 071101–4.
(58) *Chemistry WebBook*, NIST Standard Reference Database Number 69, June 2005 Release, http://webbook.nist.gov/chemistry/.

JP1047584